AMERICAN SOCIETY of
GENE & CELL
THERAPY

Exosomes Derived from miR-143-Overexpressing MSCs Inhibit Cell Migration and Invasion in Human Prostate Cancer by Downregulating TFF3

Yuanyuan Che,[1] Xu Shi,[1] Yunpeng Shi,[2] Xiaoming Jiang,[3] Qing Ai,[1] Ying Shi,[4] Fengyan Gong,[5] and Wenyan Jiang[6]

[1]Clinical Laboratory, The First Hospital of Jilin University, Changchun 130000, P.R. China; [2]Department of Hepatobiliary and Pancreatic Surgery, China-Japan Union Hospital of Jilin University, Changchun 130000, P.R. China; [3]Emergency Department, The First Hospital of Jilin University, Changchun 130000, P.R. China; [4]Department of Hepatology, The First Hospital of Jilin University, Changchun 130000, P.R. China; [5]Department of Gynaecology and Obstetrics, The First Hospital of Jilin University, Changchun 130000, P.R. China; [6]Department of Radiology, The First Hospital of Jilin University, Changchun 130000, P.R. China

Exosomes are membrane-enclosed nanovesicles that shuttle active cargoes, such as mRNAs and microRNAs (miRNAs), between different cells. Mesenchymal stem cells (MSCs) are able to migrate to the tumor sites and exert complex functions over tumor progress. We investigated the effect of human bone marrow-derived MSC (BMSC)-derived exosomal miR-143 on prostate cancer. During the co-culture experiments, we disrupted exosome secretion by the inhibitor GW4869 and overexpressed exosomal miR-143 using miR-143 plasmid. miR-143 was involved in the progression of prostate cancer via trefoil factor 3 (TFF3). Moreover, miR-143 was downregulated while TFF3 was upregulated in prostate cancer cells and tissues, and miR-143 was found to specifically inhibit TFF3 expression. Human MSC-derived exosomes enriched miR-143 and transferred miR-143 to prostate cancer cells. Furthermore, elevated miR-143 or exosome-miR-143 or silencing TFF3 inhibited the expression of TFF3, proliferating cell nuclear antigen (PCNA), matrix metalloproteinase (MMP)-2, and MMP-9 and PC3 cell proliferation, migration, invasion, and tumor growth, whereas it promoted apoptosis. In conclusion, hMSC-derived exosomal miR-143 directly and negatively targets TFF3 to suppress prostate cancer.

INTRODUCTION

Prostate cancer has become a serious threat to the life of patients. Owing to the aging and quick growth of population in the world, there is expected to be over 1.7 million people with prostate cancer by 2030 with about 499,000 new deaths.[1] Prostate cancer can be diagnosed by digital rectal examination and alteration of such biological markers as serum prostate-specific antigen (PSA).[2] However, most tools used now are not so sensitive and specific in detecting prostate cancer,[3] making it even more difficult to treat prostate cancer effectively. Although androgen-deprivation therapy is effective, the mainstream for treatment of metastatic prostate cancer at the early stage and molecular mechanisms underlying development to castration-resistant prostate cancer remain unclear.[4] Therefore, it is an urgent need to explore more treatment options to diminish the risk of prostate cancer.[5]

Mesenchymal stem cells (MSCs) are a heterogeneous subgroup of stromal stem cells, which can be self-renewed and differentiated into mesodermal lineages and other embryonic lineages.[6] Moreover, MSCs, possessing an inherent tropism for sites of inflammation, recurrently exist in sites of cancer, including prostatic lesions.[7] Additionally, MSCs are demonstrated to act as cytokines or a delivery vehicle of anti-tumor drugs to participate in the treatment of prostate cancer.[8]

Exosomes, lipid bilayer-enclosed extracellular vesicles containing proteins and nucleic acids, are secreted by cells and can circulate in the blood.[9] A previous study showed that, as extracellular vesicles, exosomes can transfer microRNAs (miRNAs), mRNAs, and proteins to regulate inflammation.[10] As a regulator of cell differentiation, proliferation, and apoptosis,[11] miR-143 has been found to exert inhibitory effects on tumors of prostate cancer recently.[12] Furthermore, it has been reported that miR-143 is loaded in exosomes in prostate cancer cells.[13] The prostate cancer-derived exosomes are observed in the prostatic secretions, urine, tissues, and blood.[14] Importantly, the aggressiveness of prostate cancer cells could be enhanced through exosomes under hypoxic conditions.[15] It is revealed that the management of the exosomes derived from MSCs can play an essential role in various diseases.[16] MSC-derived exosomes may act as suppressors of the prostate cancer-induced angiogenesis on prostate PC-3 tumor cells, and, thus, they could be suitable for anti-cancer therapies.[17] These findings underline the critical role of MSC-derived exosomal miR-143 in the progression of prostate cancer. Thus, this study explored the specific mechanism of human bone marrow-derived

MSC (BMSC)-derived exosomal miR-143 in prostate cancer cell migration and invasion.

RESULTS

hsa-miR-143 in Exosomes Influences Prostate Cancer by Regulating TFF3

We extracted prostate cancer expression profile data from the GEO database. Five prostate-related expression datasets (GEO: GSE3868, GSE30994, GSE38241, GSE46602, and GSE103512) were identified. Differential analysis of gene expression in these five datasets obtained 224, 3,000, 1,008, 759, and 276 differentially expressed genes, respectively. To further screen out prostate cancer-associated genes, Venn analysis was performed to obtain the cross-section of the differential genes in the five datasets (Figure 1A). Interestingly, only the trefoil factor 3 (TFF3) gene was shared by all five datasets. To further check the expression of the TFF3 gene in five datasets, TFF3 expression level in each dataset was analyzed, and, as shown in Figures 1B–1F, the TFF3 gene was highly expressed in prostate cancer samples in all five datasets compared with normal samples.

To investigate the upstream regulatory mechanism of the TFF3 gene, the upstream regulatory miRNAs of TFF3 were predicted; 22 TFF3 potential regulatory miRNAs were predicted in the microRNA Data Integration Portal (mirDIP) database and 212 in the TargetScan database (Figure 1G). There were 5 overlapping miRNAs between these two populations of miRNAs, and Homo sapiens (hsa)-miR-143 scored the highest among the five miRNAs predicted (Table 1).[18–20] In line with our bioinformatics analysis result, a recent study demonstrated that there is a close correlation between miR-143 and the development of prostate cancer,[21] but its detailed effects on prostate cancer remain unclear. Additionally, miR-143 has been reported to be encapsulated by exosomes, transferred in different cells.[13,22] The above studies suggest that hsa-miR-143 in exosomes and TFF3 are related to the development of prostate cancer.

TFF3 Is the Target Gene of miR-143

The expression of miR-143 in 123 prostate cancer and paracancerous tissues was detected by qRT-PCR. As shown in Figure 2A, the expression level of miR-143 was decreased in prostate cancer tissues compared to paracancerous tissues ($p < 0.05$). Moreover, the expression of miR-143 in 5 prostate cancer cells (22Rv1, VCaP, LNCaP, Du145, and PC-3) and normal human prostate epithelial cells (RWPE-1) was determined by qRT-PCR (Figure 2B). The results showed that the expression of miR-143 in 5 prostate cancer cell lines was also lower than that in the normal prostate epithelial cell line. Among all five prostate cancer cell lines, PC-3 exhibited the lowest expression level of miR-143 ($p < 0.05$); therefore, the PC-3 cell line was selected for subsequent experiments.

We used the TargetScan website to identify TFF3 as a possible target gene for miR-143 (Figure 2C). The background mRNA expression of TFF3 in RWPE-1 and PC-3 was detected by qRT-PCR first. The results showed that the mRNA expression of TFF3 in PC-3 was significantly higher than in RWPE-1 ($p < 0.05$) (Figure 2D). To further

verify its accuracy, a dual luciferase assay was performed; PC-3 cells were co-transfected with mimic-negative control (NC) and TFF3-wild-type (WT), mimic-NC and TFF3-mutation type (MUT), miR-143 mimic and TFF3-WT, and miR-143 mimic and TFF3-MUT. As shown in Figure 2E, compared with the mimic-NC group, miR-143 mimic significantly decreased the intensity of luciferase activity in the TFF3-WT group ($p < 0.05$), and it had no significant effect on the luciferase activity intensity in the TFF3-MUT group ($p > 0.05$). The results suggest that TFF3 is the target gene of miR-143.

Overexpression of miR-143 Suppresses Proliferation, Migration, and Invasion while It Enhances Apoptosis of Prostate Cancer Cells

To explore the effect of miR-143 on the biological function of prostate cancer cells, we transfected PC-3 cell lines with mimic-NC or miR-143 mimic, and the proliferation, apoptosis, migration, and invasion abilities of PC-3 were examined. The results showed that, compared with the mimic-NC group, the proliferation, migration, and invasion abilities were significantly decreased, and the apoptosis rate was significantly increased in the miR-143 mimic group ($p < 0.05$) (Figures 3A–3D).

Next, we carried out qRT-PCR to determine whether miR-143 was successfully overexpressed in prostate cancer cell line PC-3 (Figure 3E). The results implied that the expression of miR-143 was significantly upregulated after the overexpression of miR-143 in PC-3 ($p < 0.05$), which verified the results in Figures 3A–3D that the overexpression of miR-143 resulted in a change in cell phenotype. At the same time, the expression of TFF3 was detected by qRT-PCR and western blot analysis (Figure 3F). The results revealed that overexpression of miR-143 could negatively regulate the expression of TFF3. All these results showed that miR-143 overexpression could repress proliferation, migration, and invasion of prostate cancer cells; induce apoptosis; and downregulate the expression of its target gene TFF3.

Exosomes Mediate BMSC-Derived Exosome miR-143 Transmit to Prostate Cancer Cells

BMSCs were identified, and, according to the findings in fluorescence-activated cell sorting (FACS), the cells were positive for CD105, CD73, and CD90 but negative for the hematopoietic markers CD34, CD45, and HLA-DR (major histocompatibility complex, class II, DR). Besides, BMSCs possess osteogenic, adipogenic, and chondrogenic differentiation abilities (Figure S1). Further, the exosomes were isolated by differential ultra-centrifugation. Multiple approaches were adopted to characterize the physical features and molecular markers of the isolated extracellular vesicles so as to identify these as exosomes. The extracellular vesicles of BMSCs were observed by transmission electron microscopy (HT7700 Exalens, Beijing SJC Science and Trade, Beijing, China). It can be clearly observed that extracellular vesicles exhibited typical morphological features of exosomes: round or elliptical shape with a diameter range of 30–100 nm and a complete membrane structure with low density content (Figure 4A).
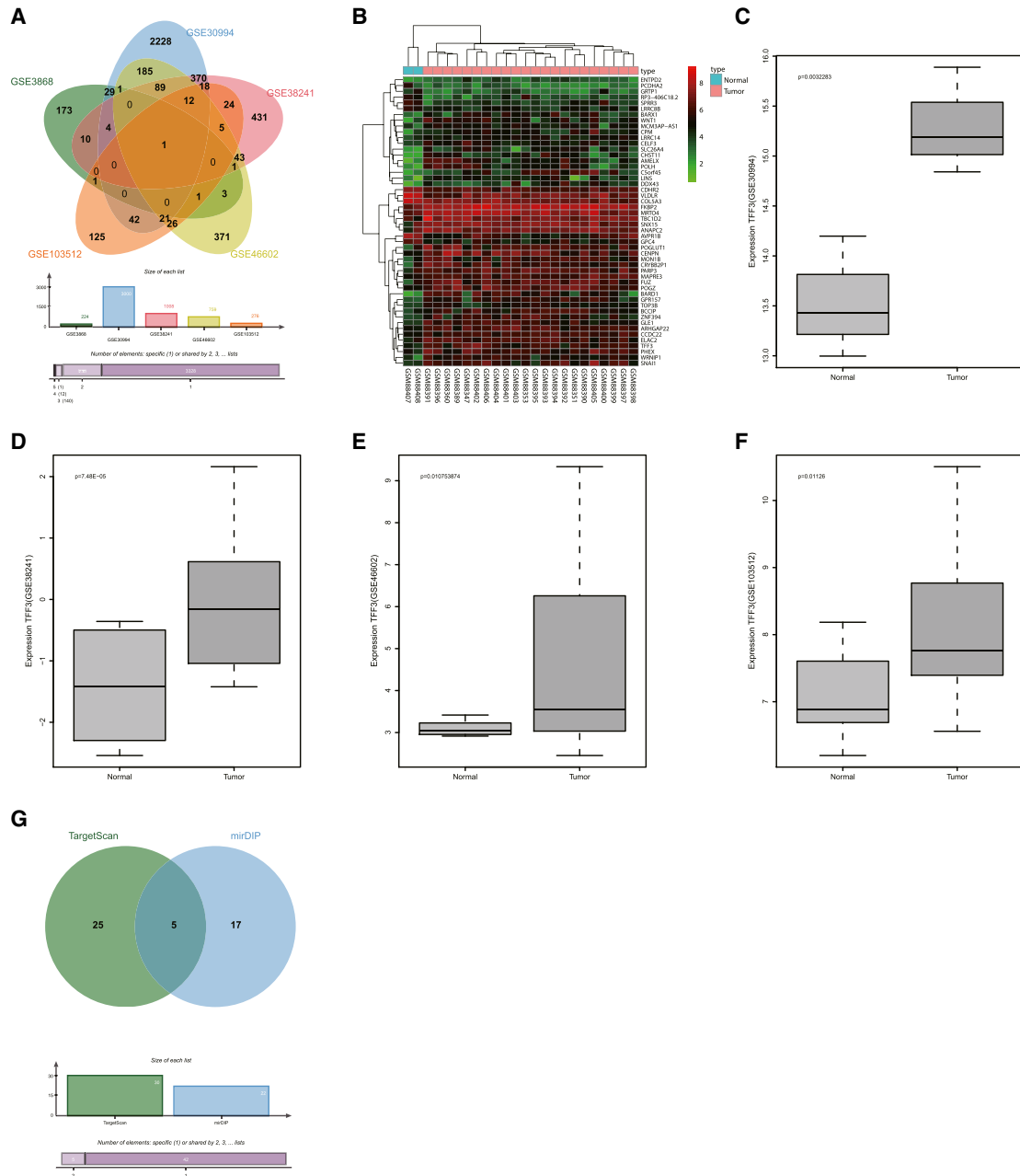
Figure 1. Screening of Prostate Cancer-Related Genes and Prediction of Their Regulatory miRNAs

(A) Venn diagram of genes shared among five prostate cancer datasets. Five different color ellipses in the figure represent the number of differential genes in five different prostate cancer datasets, and the middle part represents the cross-section of the five dataset analysis results. (B) Heatmap of the top 50 differential gene expressions in prostate cancer dataset GEO: GSE3868, in which the abscissa indicates the sample number, the ordinate indicates the gene name, the upper dendrogram indicates cluster of sample type, and the left dendrogram indicates cluster of gene expression level. Each small square in the figure represents the expression level of a gene in one sample, and the upper right histogram is a color scale. (C–F) Expression of TFF3 gene in the GEO: (C) GSE30994, (D) GSE38241, (E) GSE46602, and (F) GSE103512 expression datasets, in which the abscissa indicates the sample type, the ordinate indicates the expression level of TFF3, the left box map indicates the gene expression in the normal sample, and the right box map indicates the gene in the tumor sample. The p value is located in the upper left corner of the figure. (G) Prediction of miRNAs regulating TFF3, in which the left circle represents the top 30 miRNAs predicted in the TargetScan database, the right side represents the mirDIP database prediction results, and the middle part represents the intersection of the two database prediction results. miR-143, microRNA-143; TFF3, trefoil factor 3.

Table 1. Potential miRNA Regulating TFF3 Predicted from mirDIP and TargetScan Databases

miRNA	Integrated Score (mirDIP)	Seed Match (TargetScan)	Context++ Score Percentile (TargetScan)
hsa-miR-143	0.376788938	8-mer	99
hsa-miR-615-3p	0.309217526	8-mer	99
hsa-miR-324-5p	0.221735822	7-mer-m8	84
hsa-miR-515-3p	0.18993354	7-mer-m8	93
hsa-miR-661	0.18392694	7-mer-1A	86

miRNA/miR, microRNA; TFF3, trefoil factor 3.

Then, the nanoparticle-tracking analysis was utilized to evaluate the size distribution of extracellular vesicles, which demonstrated that the mean size of extracellular vesicles was 132.5 ± 37.4 nm and that most extracellular vesicles were distributed within the range of the exosome diameter (30–150 nm).[23,24] The most abundant extracellular vesicles were about 114 nm in diameter and the concentration was 1.8×10^{11}/L (Figure 4B). For further verification, western blot analysis was employed to assess the expressions of CD63 and TSG101 (representative markers of exosomes). As shown in Figure 4C, CD63 and TSG101 were detected in the isolated exosomes, whereas calnexin (a non-representative marker of exosomes) was not. These data demonstrated that human MSC (hMSC)-derived exosomes were successfully isolated.

Next, we compared the expression of miR-143 in hMSC-derived exosomes and BMSCs. qRT-PCR results showed that the expression of miR-143 was higher in purified exosomes than in donor BMSCs ($p < 0.05$) (Figure 4D). To explore whether the hMSC-derived exosomes could enrich miR-143 and could be adopted as a potential treatment for prostate cancer, miR-143 in BMSCs was overexpressed, separated, and purified to obtain the exo-miR-143 for subsequent experiments. As determined by qRT-PCR, the expression of miR-143 was upregulated in BMSCs treated with miR-143 compared with the BMSCs treated with miR-non-specific mimic (NSM) (Figure 4E) ($p < 0.05$). Taken together, exosomes in BMSCs can enrich miR-143.

To verify that miR-143 derived from BMSCs could be transferred to prostate cancer cells, prostate cancer PC-3 cells transduced with pCDNA3.1-GFP and BMSCs transduced with miR-143-Cy3 were co-cultured. The merged images were captured under the fluorescence microscope, and it was shown that miR-143 could be efficiently delivered into PC-3 cells via transduced BMSCs and could be delivered from donor BMSCs to recipient PC-3 cells (Figure 4F). Additionally, to study the internalization of hMSC-derived exosome miR-143 by prostate cells, hMSC-derived exosomal miR-143 was labeled with carboxyfluorescin diacetate succinimidyl ester (CFSE) fluorescent dye. The uptake of hMSC-derived miR-143 was observed under the confocal microscope.

We found that CFSE-labeled exosomes were localized in the cytoplasm, and the cellular uptake of hMSC-derived miR-143 happened

in a time-dependent manner. CFSE-labeled exosomes were incubated with the PC-3 cells for 12 h, and CFSE exosomes in PC-3 cells exhibited mild green fluorescence, indicating that the number of CFSE exosomes entering PC-3 cells was low. As time went by, more and more PC-3 cells displayed green fluorescence, and the fluorescence intensity was elevated, suggesting that the number of CFSE exosomes absorbed by PC-3 cells was increased. The uptake of CFSE exosomes by PC-3 cells was evident at 48 h (Figure 4G). Then, the miR-143 level in prostate cancer cells after 48-h incubation with CFSE exosomes was detected (Figure 4H), and the results showed that miR-143 was highly expressed in exosome-treated PC-3 cells.

To explore the role of exosomes, GW4869 was added into the co-culture system of PC-3 cells and BMSCs to reduce the secretion of exosomes. When PC-3 cells were treated with the exosome inhibitor GW4869 (Figure 4I), the miR-143 level was very low in prostate cancer PC-3 cells. Further, to confirm whether miR-143 transferred by exosomes could effectively inhibit the endogenous TFF3 in PC-3 cells, the mRNA expression of TFF3 in PC-3 cells co-cultured with BMSC miR-143 was detected using qRT-PCR, finding that BMSC miR-143 effectively suppressed the expression of TFF3 in PC-3 cells, which could be hindered by GW4869 (Figure 4J). The above results demonstrated that miR-143 could be shuttled into prostate cells by hMSC-derived exosomes.

Exosomal miR-143 Results in Declines in Prostate Cancer Cell Proliferation, Migration, and Invasion and Promotion of Apoptosis via TFF3 Downregulation

In accordance with the previous observations that miR-143 is enriched in exosomes, we assumed that miR-143 shuttled by MSC-derived exosomes could impede the proliferation, migration, and invasion in PC-3 cells. To access the role of hMSC-derived exosomes, PC-3 cells were treated with Exo-miR-NSM or Exo-miR-143, and Transwell assays were conducted. The results showed that, compared with the Exo-miR-NSM group, the proliferation, migration, and invasion abilities of the Exo-miR-143 group were significantly decreased and the apoptosis rate was significantly increased ($p < 0.05$) (Figures 5A–5D). Western blot analysis results showed (Figure 5E) that the Exo-miR-143 group had significantly decreased expression of proliferation-related factors (recombinant human Ki-67 protein [Ki67] and proliferating cell nuclear antigen [PCNA]) and invasive factors (matrix metalloproteinase [MMP]-2 and MMP-9) compared with the Exo-miR-NSM group ($p < 0.05$).

To examine the expression levels of miR-143 and TFF3 in PC-3 after Exo-miR-143 treatment, western blot analysis and qRT-PCR were conducted (Figures 5F and 5G), and the results showed that miR-143 was upregulated and TFF3 was downregulated in PC-3 in the Exo-miR-143 group when compared to the Exo-miR-NSM group ($p < 0.05$), which was consistent with our previous results. To further verify the effect of TFF3 on PC-3 cells, cell proliferation, apoptosis, migration, and invasion abilities were detected by the silencing of
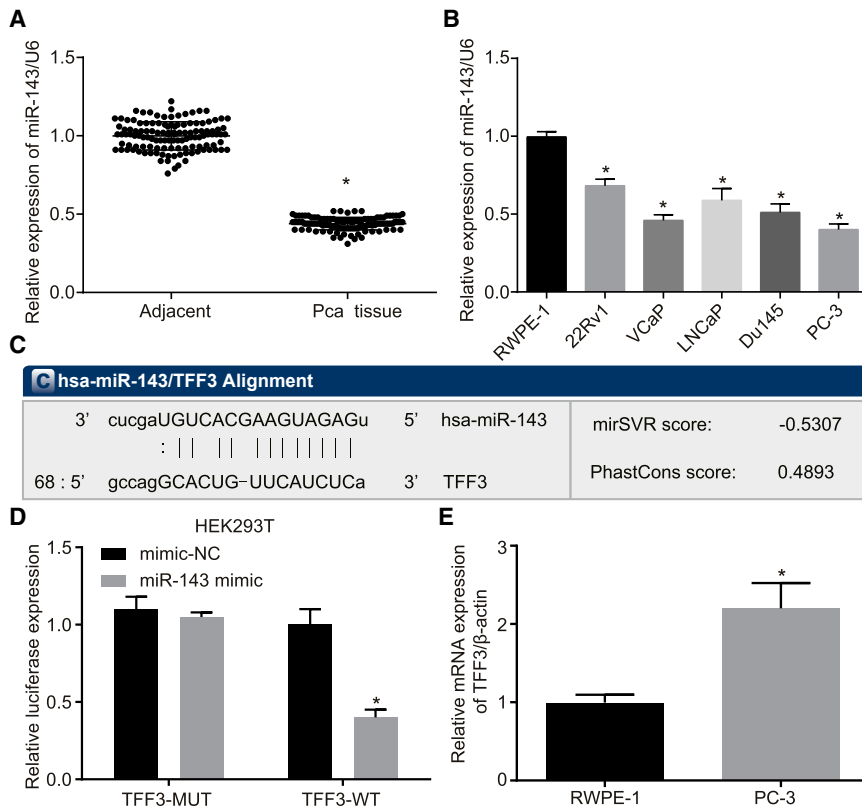
Figure 2. Prediction of the Target Gene of miR-143

(A) The expression of miR-143 in prostate cancer tissues and paracancerous tissues measured by qRT-PCR. (B) The expression of miR-143 in 5 prostate cancer cell lines and a normal cell line. (C) The binding site between miR-143 and TFF3. (D) The relative luciferase activity of luciferase reports with wild-type or mutant TFF3 were determined in PC-3 cells, which were transfected with mimic-NC or miR-143 mimic. (E) The relative mRNA expression of TFF3 in RWPE-1 and PC-3 detected by qRT-PCR. *$p < 0.05$ compared with the RWPE-1 group; the measurement data were expressed using mean ± SD, statistical analysis was performed using an independent sample t test, and the experiment was repeated three times; the t test was used for the difference analysis between two groups, while one-way ANOVA was used for multiple groups of data analysis. TFF3, trefoil factor 3; PC-3, prostate cancer cell line-3; RWPE-1, non-tumor human prostate epithelial cells.

The expression of MMP-2 in the Exo-miR-143 group was significantly reduced compared to that in the Exo-miR-NSM group; in comparison with the Si-NC group, the expression of MMP-2 in the Si-TFF3 group was also significantly decreased, which was statistically significant ($p < 0.05$) (Figure 6E). These results demonstrate that overexpression of Exo-miR-143 and silencing TFF3 can inhibit the growth and invasion of prostate cancer.

TFF3 in PC-3 (Figures 5H–5K). The results showed that, compared with the small interfering RNA (si)-NC group, the proliferation, migration, and invasion abilities of PC-3 cells in the Si-TFF3 group were significantly decreased and the apoptosis rate was significantly increased ($p < 0.05$), which were also consistent with our previous studies. Taken all together, our results confirmed that hMSC exosome-derived miR-143 can inhibit the expression of TFF3 in prostate cancer cells, further deterring prostate cancer cell proliferation, migration, and invasion, and induce apoptosis.

Exo-miR-143 and Silencing TFF3 Inhibits the Prostate Cancer Growth and Metastasis *In Vivo*

Based on the foregoing results, the role of Exo-miR-143 and TFF3 *in vivo* was evaluated by nude mice tumor formation assay. The results showed that the volume and weight of the tumor that expressed exo-miR-143 was significantly reduced ($p < 0.05$) compared to the Exo-miR-NSM group; compared with the Si-NC group, the tumor growth ability was significantly reduced, and the tumor volume was significantly reduced in the Si-TFF3 group ($p < 0.05$) (Figures 6A and 6B). At the same time, qRT-PCR was used to detect the expression of miR-143 and TFF3 in the Exo-miR-143 group (Figures 6C and 6D), and we found that, compared with the Exo-miR-NSM group, the expression level of miR-143 was significantly upregulated while the expression of TFF3 was downregulated in the Exo-miR-143 group ($p < 0.05$). Immunofluorescence staining was carried out to determine the expression of the invasion-associated factor MMP-2.

DISCUSSION

In the past few decades, prostate cancer has been at the forefront of global male malignancy mortality.[25] As for the diagnosis of prostate cancer, exponential apparent diffusion coefficient and computed diffusion-weighted imaging are often used.[26] The androgen deprivation therapy is useful in the early stage of prostate cancer, but, after the treatment, the disease can develop into castration-resistant prostate cancer.[27] However, there are few effective therapies that have been developed to cure castration-resistant prostate cancer.[28] Thus, with the expectancy to find out more effective treatment modals for prostate cancer, this study aimed at determining the roles of Exo-miR-143 and TFF3 in prostate cancer, and findings showed that the overexpression of miR-143 can inhibit proliferation, migration, and invasion and promote apoptosis of prostate cancer cells through downregulating TFF3 via BMSC-derived exosomes.

This study exhibited that miR-143 expression was decreased while TFF3 expression was increased in prostate cancer tissues and cells. A previous study disclosed that miRNAs usually showed different expression in prostate cancer patients.[29] More specifically, downregulation of miR-1 and miR-143 are usually found in prostate cancer.[30] Consistent with our study, a previous study found that TFF3 was highly expressed in prostate cancer.[31] Moreover,
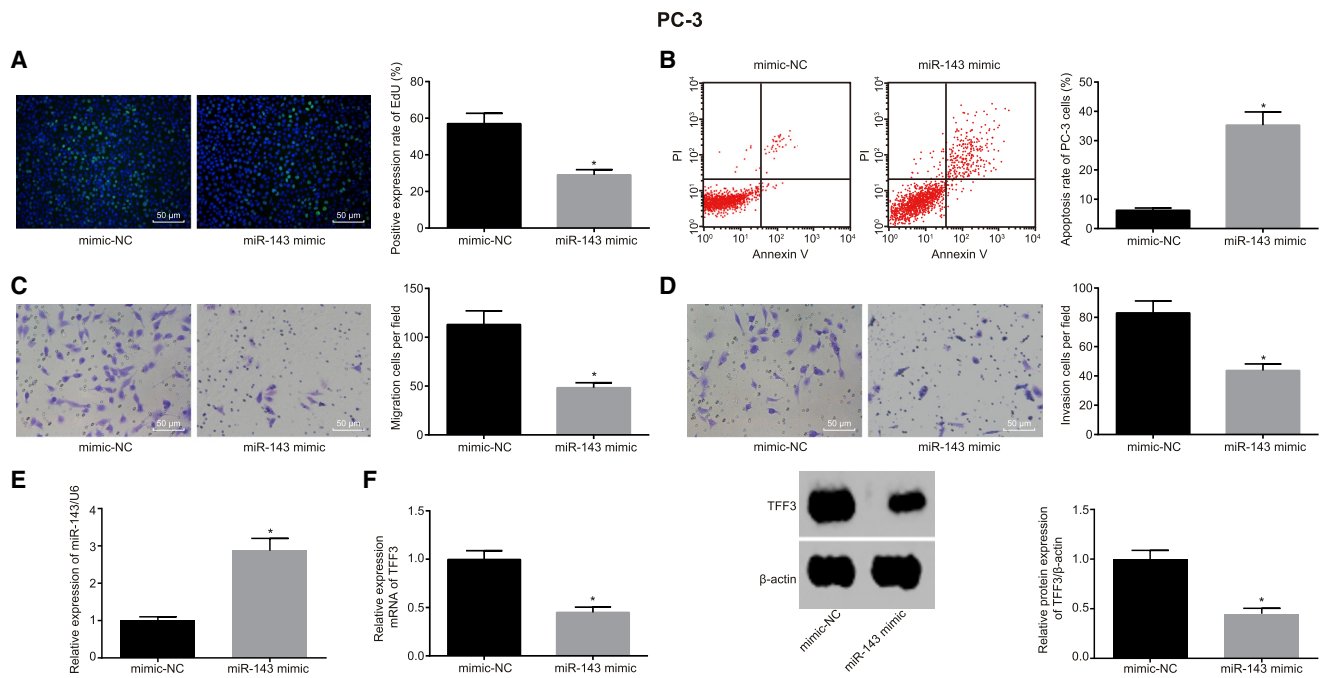
PC-3

Figure 3. Overexpression of miR-143 Affects Proliferation, Migration, Invasion, and Apoptosis in Prostate Cancer Cells
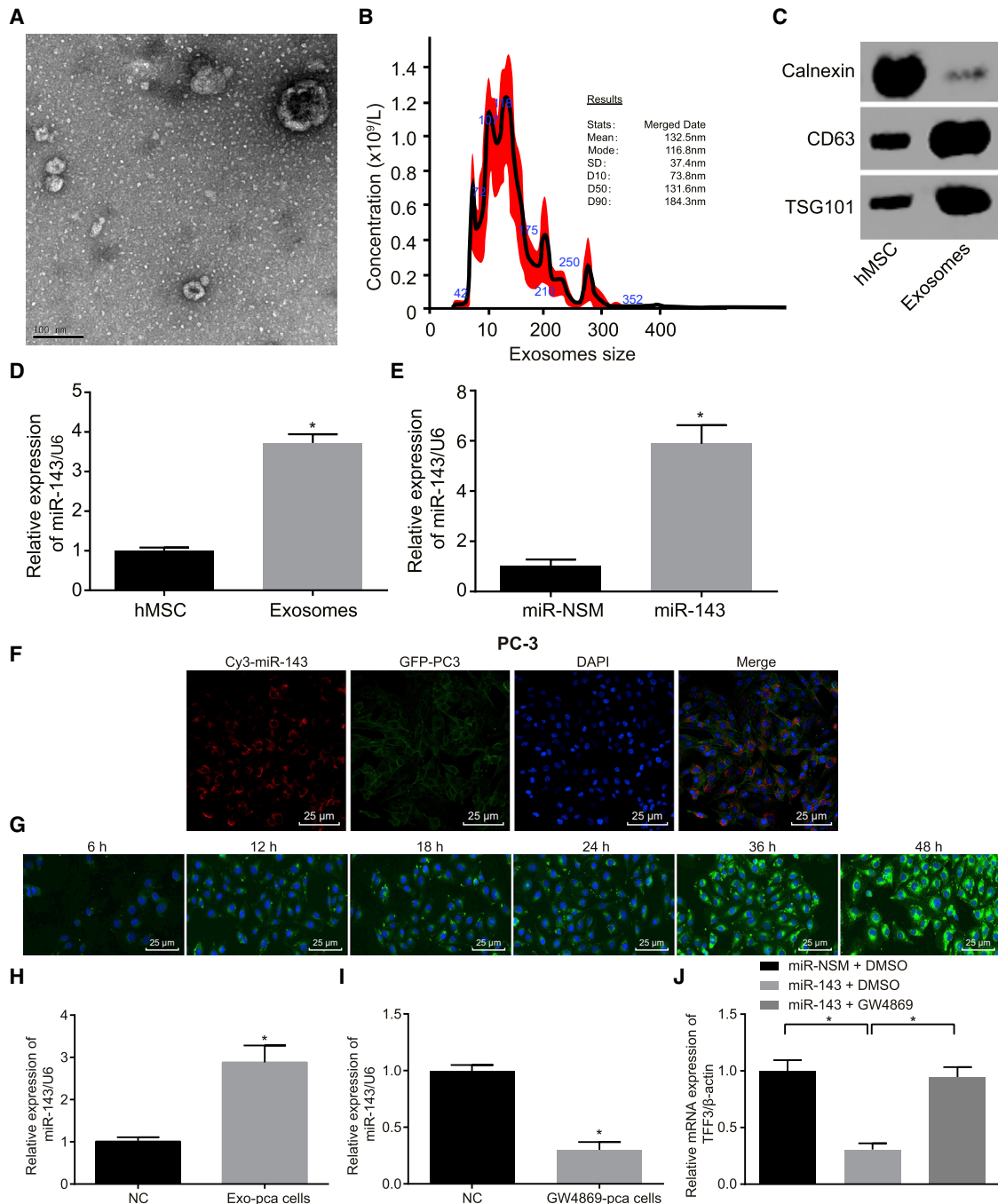
(A) The effect of overexpressed miR-143 on the proliferation of PC-3 cells determined by EdU assay (scale bar, 50 μm). (B) The apoptosis rate of PC-3 cells with overexpressed miR-143 by flow cytometry. (C) The effect of overexpressed miR-143 on the migration of PC-3 detected by Transwell assay (scale bar, 50 μm). (D) The effect of overexpressed miR-143 on the invasion of PC-3 detected by Transwell assay (scale bar, 50 μm). (E) The expression of miR-143 after overexpressing miR-143 in PC-3, measured by qRT-PCR. (F) The effect of overexpressed miR-143 on the expression of TFF3, determined by qRT-PCR and western blot analysis. *$p < 0.05$ compared with the corresponding mimic-NC group; the measurement data were expressed using mean ± SD; statistical analysis was performed using an independent sample t test, and the experiment was repeated three times. PC-3, prostate cancer cell line-3; EdU, 5-ethynyl-2′-deoxyuridine; TFF3, trefoil factor 3; NC, negative control.

TFF3 was found to be targeted by miR-143, which could mediate TFF3 expression. A previous study found that, in inflammatory bowel disease, TFF3 can be silenced by miR-7-5p.[32] It has been proven that plasminogen activator inhibitor-1, which can inhibit invasion and lung metastasis in human osteosarcoma, is a target gene of miR-143.[33] Another study showed that GLI-Kruppel family member 3 gene is also a target gene of miR-143.[34] In our study, miR-143 has been verified to specially target TFF3 by dual luciferase reporter gene assay.

In addition, our findings provide evidence that the overexpression of Exo-miR-143 and silencing of TFF3 inhibit proliferation, invasion, and migration while enhancing the apoptosis of prostate cancer, which was further verified by the decline in the expressions of PCNA, MMP-2, and MMP-9 in cells treated with Exo-miR-143. miR-143 can be encapsulated by exosomes, thus functioning in different cells.[13,22] Besides, previous studies suggest that exosomes can be derived from hMSCs.[35,36] Expressed in the nuclei of cells, PCNA is a protein that plays a major role in DNA replication.[37] It has been proven that there is a close correlation between the expression of PCNA and cell proliferation.[38] MMP-2 and MMP-9 are associated with the progression, invasion, and metastasis of malignant tumors.[39] The present study, highlighted that, when miR-143 was overexpressed, the expressions of MMP-2, PCNA, and MMP-9 were diminished, indicating the suppressive effect of miR-143 on cell invasion and proliferation in prostate cancer.

Furthermore, results obtained from a study proved that, by upregulating miR-143, curcumin can suppress prostate cancer cell migration and proliferation.[40] Also, a previous study showed that miR-143 can be regarded as an inhibitor of prostate cancer via regulating hexokinase 2.[41] Interestingly, in line with our study, another research further proved that, when TFF3 expression was decreased, castration-resistant prostate cancer cell exhibited suppressive cell invasion.[42] Another study showed that, in prostate cancer, the poor expression of TFF3 can contribute to a declined total cell number and repressed cell viability, proliferation, and survival.[43] At the same time, our study proved that miR-143 increased prostate cancer cell apoptosis. A previous study indicated that increased apoptosis was observed in prostate cancer cells following miR-143 overexpression.[44] Another study found that miR-143 induces apoptosis of hepatoma cells by regulating the nuclear factor κB (NF-κB) pathway.[45] Besides, miR-143 exerts promoter functions over the apoptosis of prostate cancer cells by mediating the expression of Bcl-2, which has been previously proven in a study.[46]
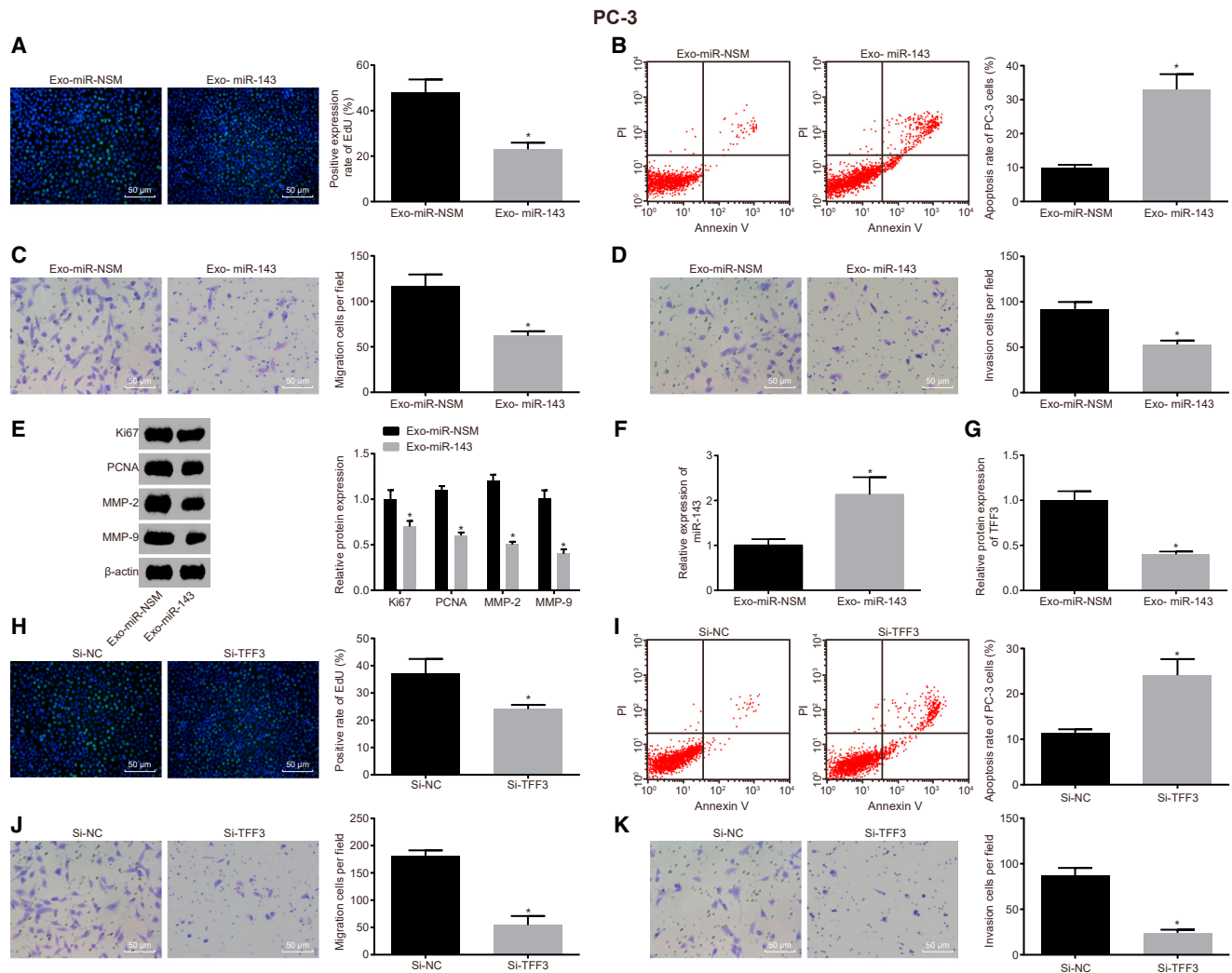
Figure 4. Exosome Isolation and Characterization in BMSCs

(A) Observation of the morphology of exosomes under a transmission electron microscope (scale bar, 100 nm). (B) The size distribution of exosomes. (C) The expression of exosomal markers CD63 and TSG101. (D) The miR-143 expression in BMSCs and hMSC-derived exosomes. (E) The miR-143 expression in BMSCs treated with miR-NSM and miR-143 detected by qRT-PCR. (F) Representative images of miR-143 delivery to PC-3 cells via BMSCs. Red, miR-143-Cy3; green, PC-3 cells; blue, DAPI-stained nucleus (scale bar, 25 μM). (G) The uptake of hMSC-derived exosomes by prostate cancer cells at different time points. Green, CFSE-labeled exosomes (scale bar, 25 μM). (H) The level of miR-143 in prostate cells after 48-h incubation with hMSC-derived exosomes. (I) miR-143 expression in prostate cells treated with the exosome inhibitor GW4869, determined by qRT-PCR. (J) qRT-PCR analysis depicting the changes of TFF3 expression level. GW4869, an inhibitor of neutral sphingomyelinase-2. *p < 0.05; the data among multiple groups were analyzed using one-way ANOVA and the data between two groups were tested by independent sample t test, and the experiment was repeated three times. BMSCs, human bone marrow-derived MSCs; DAPI, 4'-6-diamidino-2-phenylindole; NC, negative control; TFF3, trefoil factor 3.

Figure 5. Exosomal miR-143 Regulates Proliferation, Migration, Invasion, and Apoptosis via TFF3 in Prostate Cancer Cells

(A) The effect of exosomal miR-143 on the proliferation of PC-3 cells, determined by EdU assay (scale bar, 50 μM). (B) The apoptosis rate of PC-3 affected by exosomal miR-143, detected by flow cytometry. (C) The effect of exosomal miR-143 on the migration ability of PC-3, detected by Transwell assay (scale bar, 50 μM). (D) The effect of overexpressed Exo-miR-143 on PC-3 invasion ability, detected by Transwell assay (scale bar, 50 μM). (E) The expression levels of cell proliferation factors (Ki67 and PCNA) and invasive factors (MMP-2 and MMP-9). (F) The expression of miR-143 in PC-3. (G) The expression of TFF3 in PC-3. (H) The effect of silencing TFF3 on the proliferation of PC-3, detected by EdU staining. (I) The effect of silencing TFF3 on the apoptosis rate of PC-3, detected by flow cytometry. (J) The effect of silencing TFF3 on migration ability of PC-3, detected by Transwell assay (scale bar, 50 μM). (K) The effect of silencing TFF3 on the invasion ability of PC-3, detected by Transwell assay (scale bar, 50 μM). *$p < 0.05$ compared with the Exo-miR-NSM group (A–G); *$p < 0.05$ compared with the Si-NC group (H–K); the measurement data were measured using mean ± SD; an independent sample t test was used for statistical analysis between the two groups, and the experiment was repeated three times. EdU, 5-ethynyl-2′-deoxyuridine; TFF3, trefoil factor 3; PC-3, prostate cancer cell line-3; PCNA, proliferating cell nuclear antigen; MMP, matrix metalloproteinase; NC, negative control.

Based on the previous research, our results demonstrated that overexpressed miR-143 exerts suppressive effects on prostate cancer by downregulating TFF3 (Figure 7). These findings identify miR-143 and the TFF3 gene as potential therapeutic targets for the treatment of prostate cancer. It is also recommended that a larger *in vivo* experiment should be carried out in further studies to completely understand the underlying mechanism of miR-143 and the TFF3 gene in prostate cancer.

MATERIALS AND METHODS
Ethics Statement

During the animal experiment, the guidelines for the protection and use of experimental animals issued by the NIH in the United States were strictly observed, and the principle of completing the experiment with the minimum number of animals and minimizing the pain of the experimental animals was strictly observed. The study was also approved by the Institutional Review Board of The First Hospital of
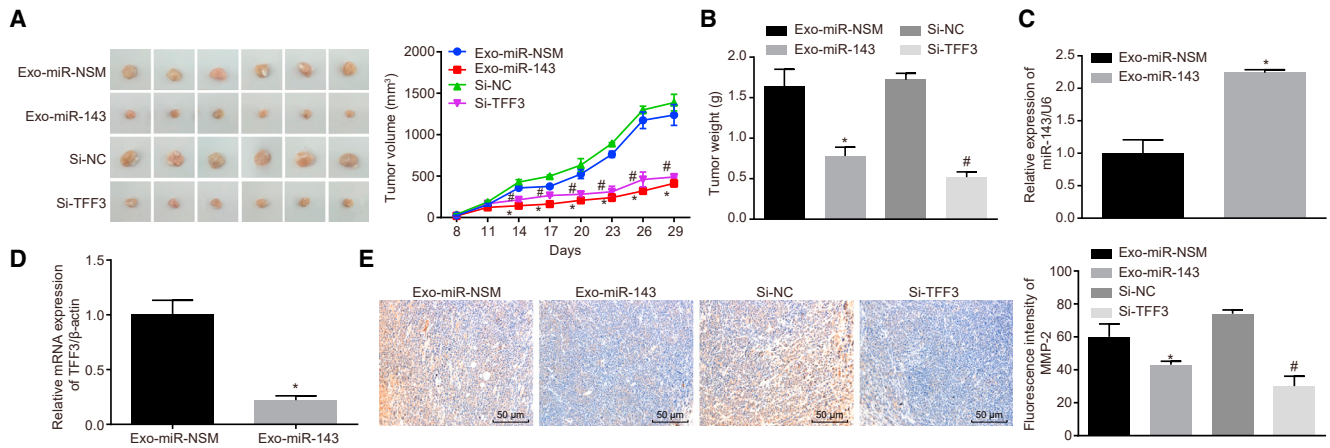
Figure 6. Exo-miR-143 and Silencing TFF3 Affect Tumor Growth and Metastasis of Prostate Cancer *In Vivo*

(A) Photographs of tumor and curve of tumor volume growth for the nude mice. (B) Tumor weight. (C) The expression of miR-143 detected by qRT-PCR. (D) The expression of TFF3 in tumors, detected by qRT-PCR. (E) The expression of invasion-related factor MMP-2 in each group, detected by immunofluorescence (scale bar, 50 μM). *$p < 0.05$ compared with the Exo-miR-NSM group; #$p < 0.05$ compared with the Si-NC group; the measurement data were measured using mean ± SD, and the independent sample t test was used for statistical analysis; N = 6. MMP, matrix metalloproteinase; TFF3, trefoil factor 3; NC, negative control.

Jilin University. Written informed consent was obtained from each participant.

Bioinformatics Analysis

We searched the GEO database (https://www.ncbi.nlm.nih.gov/geo/) for prostate cancer-related expression datasets, and the limma package in the R language was used for differential analysis of the prostate cancer datasets, with |logFC| > 2 and p < 0.05 set as the screening threshold. The differential gene expression heatmap was constructed using the pheatmap package.

The miRNAs regulating the TFF3 gene were predicted using the TargetScan database (http://www.targetscan.org/vert_71/) and the mirDIP database (http://ophid.utoronto.ca/mirDIP/index.jsp#r). The Venn diagram was employed to obtain the intersection of the two database prediction results.

Clinical Prostate Samples and Cell Lines

A total of 123 clinical samples of prostate cancer and corresponding paracancerous tissues was collected from patients who received treatment at The First Hospital of Jilin University from September 2015 to September 2017. Human BMSCs, five prostate cancer cell lines (22Rv1, VCaP, LNCaP, Du145, and PC-3), and normal prostate epithelial cells RWPE-1 were provided by the Cell Resource Center of the Institute of Basic Medical Sciences, Chinese Academy of Medical Sciences (Beijing, China). The cells were cultured in RPMI-1640 (Gibco, Carlsbad, CA, USA) medium supplemented with 10% fetal bovine serum (FBS), 100 μg/mL streptomycin, and 100 U/mL penicillin at 37°C with 5% CO_2 and 95% saturated humidity. The culture liquid was exchanged 3–4 times every week based on the growth of cultured cells. When cell confluence reached about 80%, cells were sub-cultured. Afterward, the expression of miR-143 in 5 prostate cancer cell lines was measured using qRT-

PCR, and the cell line with lowest miR-143 expression was selected for subsequent experiments.

BMSC Identification

The BMSCs at passage 3 in good growth state were detached and the concentration was adjusted into 5×10^4 cells/mL, which were then inoculated into the 6-well plate pre-covered with cover glass. After 24 h, the BMSCs completely adhered to the wall. After that, BMSCs were incubated for 4 weeks using MSC Osteogenic Differentiation Medium Kit (Cyagen, Silicon Valley, CA, USA) and Adipogenic Differentiation Medium Kit (Cyagen, Silicon Valley, CA, USA). Next, the BMSCs were stained in order to determine the abilities of osteogenic and adipogenic differentiation in strict conformity to the protocols of the kits. Subsequently, the images were obtained under a microscope (CK40, Olympus, Tokyo, Japan). The markers of BMSCs were identified using flow cytometry. Antibodies fluorescein isothiocyanate (FITC)-CD105, FITC-CD73, phycoerythrin (PE)-CD90 (Abcam, Cambridge, UK), CD34, CD45 (PE, eBioscience, Thermo Fisher Scientific, Waltham, MA, USA), and PE-HLA-DR (Abcam, Cambridge, UK) were added to different test tubes according to the specifications of antibodies, and immunoglobulin G (IgG) FITC or IgG (Abcam) served as the homologous control.

Cell Culture and Transfection

The transfection of BMSCs was classified into miR-NSM group, miR-143 mimic group, and mimic-NC group. RNA duplexes corresponding to hsa-miR-143 were initially marked with Cy3 (Life Technologies, Gaithersburg, MD, USA). The transfection of PC-3 was assigned into the si-TFF3 group, si-negative control (NC) group, miR-143 mimic group, and mimic-NC group. For the transfection, the target plasmids were purchased from Vigene Biosciences (Rockville, MD, USA). The transfection was performed using the Lipofectamine 2000 (Invitrogen, Carlsbad, CA, USA) kit based on the
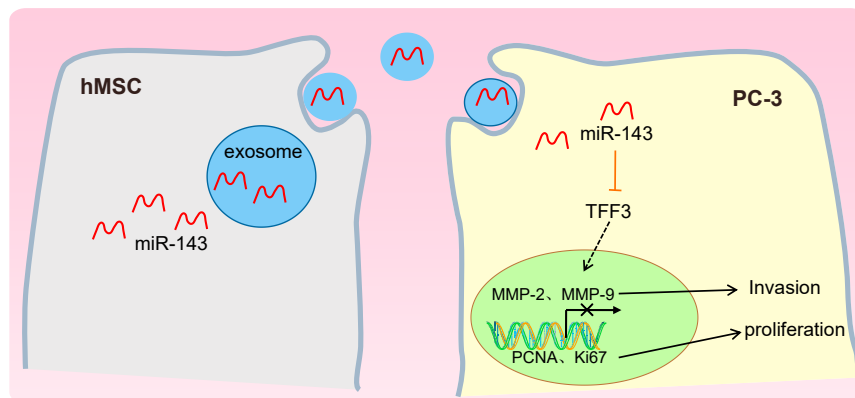
Figure 7. Mechanism of hMSC-Derived Exo-miR-143 as a Potential Treatment for Prostate Cancer

miR-143 was poorly expressed in PC-3 cells while TFF3 was highly expressed. miR-143 can inhibit the proliferation, migration, and invasion and promote apoptosis in prostate cancer cells by negatively mediating the expression of the TFF3 gene. Thus, hMSC-derived Exo-miR-143 could be a potential treatment for prostate cancer.

manufacturer's instructions. Briefly, 4 µg target plasmid and 10 µL Lipofectamine 2000 were respectively diluted using 250 µL Opti-MEM medium (Gibco, Carlsbad, CA, USA). After that, the mixture was allowed to stand for 20 min at room temperature, and then it was added into the cell culture wells for incubation at 37°C with 5% CO_2. After 6 h, the medium was replaced. Then, the cells were collected for subsequent experiments after another 36– to 48-h incubation.

Dual Luciferase Reporter Assay

To confirm whether TFF3 is the direct target gene of miRNA-143, the synthetic 3′ UTR fragment of TFF3 was inserted into the 3′ UTR of luciferase gene pMIR-reporter (Beijing Huayueyang Biotechnology, Beijing, China) to construct a TFF3-WT vector. The mutation site of the 3′ UTR fragment of TFF3 was inserted into the 3′ UTR of the luciferase gene pMIR-reporter (Beijing Huayueyang Biotechnology, Beijing, China) to construct the TFF3-MUT vector. The luciferase reporter plasmids containing TFF3-WT or TFF3-MUT were co-transfected with miR-143 into HEK293T, respectively. Renilla luciferase was served as an internal reference. After transfection for 48 h, the cells were collected and lysed. The luciferase activity was measured using Luciferase Detection kit (K801-200, BioVision, San Francisco, CA, USA) Glomax 20/20 luminometer fluorescence detector (Promega, Madison, WI, USA). The experiment was repeated three times.

qRT-PCR

Total RNA was obtained from tissues or cells using Trizol (Invitrogen, Carlsbad, CA, USA). RNA concentration was measured by Nanodrop 2000 (Thermo Fisher Scientific, MA, USA); 1 µg total RNA was reversely transcribed into cDNA using PrimeScript RT reagent kit (Takara Holdings, Kyoto, Japan). Real-time PCR was carried out on an ABI7500 qPCR machine (Thermo Fisher Scientific, MA, USA) using the SYBR Premix Ex Taq (Tli RNaseH Plus) kit (Takara Holdings, Kyoto, Japan). The PCR-cycling conditions were as follows: one cycle pre-denaturation at 95°C for 10 min, and 40 cycles denaturation at 95°C for 15 s and annealing at 60°C for 30 s. β-actin served as an internal reference of TFF3, and U6 was used as an internal reference of miR-143. The $2^{-\Delta\Delta Ct}$ method was adopted to calculate the ratio of target gene expression in the observation group to that in the reference group. The primers used in the reaction are shown in Table 2, and the primers were all supplied by Shanghai GenePharma (Shanghai, China). The experiment was repeated three times.

Western Blot Analysis

The total protein was obtained from each group of cells, and the protein concentration was determined using a BCA protein assay kit (Thermo Fisher Scientific, MA, USA). Total protein (30 µg) was subjected to polyacrylamide gel electrophoresis at a constant voltage of 80 V for 35 min and 120 V for 45 min and transferred onto a polyvinylidene fluoride (PVDF) membrane (GE Healthcare, Chicago, IL, USA). The membrane was blocked for 1 h with 5% skim milk at room temperature. After that, the membrane was incubated at 4°C overnight with CD63 rabbit monoclonal antibody (1: 1,000, ab134045), tumor susceptibility gene 101 (TSG101) rabbit monoclonal antibody (1:1,000, ab125011), calnexin rabbit polyclonal antibody (1:1,000, ab22595), Ki67 rabbit monoclonal antibody (1:5,000, ab92742), PCNA rabbit polyclonal antibody (1:1,000, ab18197), MMP-2 rabbit monoclonal antibody (1:1,000, ab37150), MMP-9 rabbit polyclonal antibody (1:1,000, ab73734), and β-actin rabbit polyclonal antibody (1:5,000, ab8227). All the aforementioned antibodies were purchased from Abcam (Cambridge, UK). Afterward, the membrane was incubated with horseradish peroxidase-labeled goat anti-rabbit secondary antibody (1:10,000, Jackson ImmunoResearch Laboratories, West Grove, PA, USA) for 1 h at room temperature and developed under an optical luminometer (GE Healthcare, Chicago, IL, USA). Subsequently, the intensity of each band was read and analyzed with Image Pro Plus 6.0 software (Media Cybernetics, MD, USA). The experiment was repeated three times.

EdU Assay

The 5-ethynyl-2′-deoxyuridine (EdU) assay was set up to assess cell proliferation. The prostate cancer cell line PC-3 was incubated with EdU solution (the cell culture medium and the EdU solution were mixed at a ratio of 1,000:1) at room temperature for 2 h and rinsed with PBS. The cell culture plate was fixed with 40 g/L paraformaldehyde for 30 min, incubated with glycine solution for 8 min, washed with PBS, and then rinsed with PBS containing 0.5% Triton X-100. With an addition of Apollo staining reaction solution, the culture plate was incubated at room temperature under conditions void of

Table 2. Primer Sequence for qRT-PCR

Gene	Primer Sequence
miR-143	F: 5′-AGTCAGTGAGATGAAGCACTG-3′
	R: 5′-GTGCAGGGTCCGAGGT-3′
U6	F: 5′-AGAGCCTGTGGTGTCCG-3′
	R: 5′-CATCTTCAAAGCACTTCCCT-3′
β-actin	F: 5′-CGGGACCTGACTGACTACCTC-3′
	R: 5′-CCATCTCTTGCTCGAAGTCCAG-3′
TFF3	F: 5′-CTCCAGCTCTGCTGAGGAGT-3′
	R: 5′-CAGGGATCCTGGAGTCAAAG-3′

TFF3, trefoil factor 3; miR-143, microRNA-143; F, forward; R, reverse.

light and washed two times with methanol and PBS, respectively. After being added with Hoechst 3334 reaction solution and incubated at room temperature for 20 min under conditions void of light, the cell was observed under the fluorescence microscope. The green-stained cells were proliferating cells. When photographed in the purple light of the excitation channel, the blue-stained cells were the total cells. Three fields were randomly chosen, and EdU-stained cells (proliferating cells) and Hoechst 33342-stained cells (total cells) were counted (cell proliferation rate = number of proliferating cells/total number of cells × 100%). The experiment was repeated three times.

Transwell Assay
Transwell assay was performed using 24-well chambers containing membrane filter inserts. After 48 h of transfection, the prostate cancer cell line PC-3 was serum-starved for 24 h, detached, and washed two times with PBS. After centrifugation, the cells were counted and resuspended in serum-free RPMI1640 medium supplemented with 10 g/L BSA at the cell density of 3×10^4 cells/mL. The Transwell chambers or chambers coated with Matrigel (40111ES08, Yeasen, Shanghai, China) were used for the migration assay or invasion assay, respectively. After conventional detachment, the cells were rinsed two times with PBS and resuspended with RPMI1640 medium at the cell density adjusted to 1×10^5 cells/mL. A total of 200 μL cell suspension was added to the apical chamber of the Transwell chamber. RPMI1640 medium (600 μL) supplemented with 20% FBS was added into the basolateral chamber. After 24 h of conventional culture, the Transwell chamber was removed, and the cells on the inner surface of the apical chamber were removed with a cotton swab. Afterward, the cells that migrated into the lower side of the membrane were fixed with 4% paraformaldehyde for 15 min, stained with 0.5% crystal violet solution for 15 min, and washed 3 times with PBS. Micrographs were acquired with an inverted microscope (XDS-800D, Shanghai Caikon Optical Instrument, Shanghai, China), and the transmembrane cells were counted in a number of random fields. Three replicate wells were set up in each assay. The experiment was repeated 3 times.

Flow Cytometry
The apoptosis of cells was detected using Annexin V-FITC-propidium iodide (PI) double-labeled staining. The cells were collected

48 h after transfection and prepared 1×10^6 cells/mL cell suspension. The cells were then fixed with a pre-cooled 70% ethanol solution at 4°C overnight and washed two times with PBS. The cell suspension (100 μL, cells not less than 1×10^6 cells/mL) was washed two times with PBS and centrifuged. Subsequently, the cells were resuspended in 200 μL binding buffer, 10 μL Annexin V-FITC, and 5 μL PI, and they were incubated at room temperature for 15 min under conditions void of light. Cell apoptosis was detected by flow cytometer at an excitation wavelength of 488 nm.

Co-culture of BMSCs and PC-3 Cells
Prostate cancer cell line PC-3 was transfected with fluorescence-labeled pCDNA3.1-GFP, and BMSCs were transduced with Cy3-labled miR-143 (miR-143-Cy3). After treatment, PC-3 cells and BMSCs were blended (1: 1) and then inoculated into a 96-well plate, with 100 cells in each well for co-culture for 2 days. After that, the mixture was separated using flow cytometry, followed by analysis using the fluorescence microscope. Subsequently, the specific inhibitor GW4869 (Sigma, St. Louis, MO, USA) was added in order to block the release of exosomes. To confirm that miR-143 was delivered via exosomes, cells were manipulated with GW4869 or DMSO, with DMSO as a negative control. Next, the cells were re-inoculated in the 6-well plate for co-culture with the tumor cells for 48 h with 10 M GW4869 or DMSO.

Exosome Isolation
Exosomes were separated by ultracentrifugation-based isolation techniques.[47] Exosomes were harvested with ultracentrifugation. Briefly, BMSCs were grown to approximately 80% before culturing in exosome-free medium for 48 h. Exosome-free medium was prepared using FBS and centrifuged for 8 h at $100,000 \times g$. Then the culture supernatant was centrifuged at $300 \times g$ for 10 min at 4°C, at $2,000 \times g$ for 15 min, at $5,000 \times g$ for 15 min, and at $12,000 \times g$ for 30 min. After centrifugation, the supernatant was collected. The supernatant was ultra-centrifuged at $100,000 \times g$ for 70 min to pellet the exosomes. Exosomes were washed with PBS and pelleted by ultracentrifugation for 70 min at $100,000 \times g$. All ultracentrifugation steps were performed at 4°C in a Beckman ultracentrifuge (TL-100) with TLS-55 swinging bucket rotor. The rest of the low-speed centrifuges utilized Beckman Allegra X-15R centrifuges.[48]

Nanoparticle-Tracking Analysis
Nanoparticle-tracking analysis was employed to determine the size of exosomes. Exosomes (20 μg) were dissolved in 1 mL PBS and vortexed for 1 min with the exosomes evenly distributed. Then, the scale distribution of exosomes was measured and observed using the NanoSight Nanoparticle Tracking Analyzer (NTA, Malvern Panalytical, UK).

Transmission Electron Microscope
The exosomes were immediately fixed with 4% glutaraldehyde for 2 h at 4°C after isolation, washed 3 times with 0.1 mol/L PBS, fixed with 1% osmium tetroxide for 2 h, and dehydrated with conventional ethanol and acetone. Exosomes was impregnated with epoxy resin, embedded, and polymerized. After that, 0.5-μm-thick semi-thin sections were prepared, and the ultra-thin sections of 60 nm were

prepared after localization of the light microscope. The sections were stained with uranium acetate and lead citrate and visualized under an electron microscope.

Cellular Uptake of Exosomes
Exosomes (20 μg) were labeled with CFSE dye, which was diluted at a ratio of 1:1,000. After 15-min incubation at 37°C, the exosomes were harvested and washed with PBS by centrifugation ($100,000 \times g$, 70 min). CFSE-tagged exosomes were added to prostate cancer cells and incubated for 6, 12, 18, 24, 36, and 48 h at 37°C, and cellular uptake was observed under a confocal fluorescence microscope.

Tumor Formation in Nude Mice
The 24 4-week-old BALB/C male nude mice were provided by Hunan SJA Laboratory Animal (Hunan, China). The nude mice were divided into 4 groups with 6 mice in each group at random for tumor growth observation. PC-3 cells were treated with exosomes (Exo)-miR-NSM and Exo-miR-143 (PC-3/Exo-miR-NSM group and PC-3/Exo-miR-143 group) and transfected with Si-NC and Si-TFF3, respectively (PC-3/Si-NC group and PC-3/Si-TFF3 group). The cells of each group were then resuspended in 50% Matrigel (BD Biosciences, Franklin Lakes, NJ, USA). A total of 0.2 mL cells (1×10^6 cell/mL) was subcutaneously injected into the flanks of mice. The tumor size was measured with a vernier caliper every 3 days since day 8 after injection, and then the tumor volume (mm³) was calculated using the following formula: tumor volume = length $\times$ width^2 $\times$ 0.5. After 30 days of tumor cell implantation, all nude mice were sacrificed, and the tumor was removed and weighed. miR-143 and TFF3 expression levels in the PC-3/Exo-miR-NSM group and the PC-3/Exo-miR-143 group were detected by qRT-PCR.

Immunohistochemistry
The nude mice were anesthetized by intraperitoneal injection of 0.1 mL 1% sodium pentobarbital, and the solid tumors were quickly removed. The tumor tissues were fixed in paraformaldehyde for 48–72 h, embedded in paraffin, and cut into sections at 5 μm. The sections were dewaxed with xylene, dehydrated with alcohol, and blocked endogenous peroxidase with 3% hydrogen peroxide. After antigen retrieval, the sections were added with primary antibody MMP-2 (1:1,000, ab37150, Abcam, Cambridge, UK) for 1-h incubation at 37°C and horseradish peroxidase-labeled secondary antibody (1:1,000, ab6721, Abcam, Cambridge, UK) at 37°C for 30 min. The color was developed using freshly prepared diaminobenzidine (DAB) solution for 1–2 min; rinsed 2 min, 3 times with PBS; and counterstained with hematoxylin for 1 min. The staining was observed under an optical microscope.

Statistical Analyses
Statistical analyses were conducted with SPSS 21.0 statistical software (IBM, Armonk, NY, USA). The data were expressed as mean ± SD. The difference between two groups was analyzed by t test and corrected by Welch. Normality test among multiple groups was conducted by the Shapiro-Wilk method. One-way ANOVA was used for the data subject to normal distribution. Least-significant difference (LSD) was used to compare difference among multiple groups. A non-parametric Kruskal-Wallis test was used for comparison between data that did not conform to normal distribution. p values < 0.05 were considered statistically significant.

SUPPLEMENTAL INFORMATION
Supplemental Information can be found online at https://doi.org/10.1016/j.omtn.2019.08.010.

CONFLICTS OF INTEREST
The authors declare no competing interests.

REFERENCES
1. Center, M.M., Jemal, A., Lortet-Tieulent, J., Ward, E., Ferlay, J., Brawley, O., and Bray, F. (2012). International variation in prostate cancer incidence and mortality rates. Eur. Urol. 61, 1079–1092.

2. Kalsbeek, A.M.F., Chan, E.K.F., Grogan, J., Petersen, D.C., Jaratlerdsiri, W., Gupta, R., Lyons, R.J., Haynes, A.M., Horvath, L.G., Kench, J.G., et al. (2018). Altered mitochondrial genome content signals worse pathology and prognosis in prostate cancer. Prostate 78, 25–31.

3. Shao, X., Pan, J., Wang, Y., Zhu, Y., Xu, F., Shangguan, X., Dong, B., Sha, J., Chen, N., Chen, Z., et al. (2017). Evaluation of expressed prostatic secretion and serum using surface-enhanced Raman spectroscopy for the noninvasive detection of prostate cancer, a preliminary study. Nanomedicine (Lond.) 13, 1051–1059.

4. Abd Elmageed, Z.Y., Yang, Y., Thomas, R., Ranjan, M., Mondal, D., Moroz, K., Fang, Z., Rezk, B.M., Moparty, K., Sikka, S.C., et al. (2014). Neoplastic reprogramming of patient-derived adipose stem cells by prostate cancer cell-associated exosomes. Stem Cells 32, 983–997.

5. Cui, K., Li, X., Du, Y., Tang, X., Arai, S., Geng, Y., Xi, Y., Xu, H., Zhou, Y., Ma, W., and Zhang, T. (2017). Chemoprevention of prostate cancer in men with high-grade prostatic intraepithelial neoplasia (HGPIN): a systematic review and adjusted indirect treatment comparison. Oncotarget 8, 36674–36684.

6. Si, Y.L., Zhao, Y.L., Hao, H.J., Fu, X.B., and Han, W.D. (2011). MSCs: Biological characteristics, clinical applications and their outstanding concerns. Ageing Res. Rev. 10, 93–103.

7. Brennen, W.N., Denmeade, S.R., and Isaacs, J.T. (2013). Mesenchymal stem cells as a vector for the inflammatory prostate microenvironment. Endocr. Relat. Cancer 20, R269–R290.

8. Yan, F., Li, X., Li, N., Zhang, R., Wang, Q., Ru, Y., Hao, X., Ni, J., Wang, H., and Wu, G. (2017). Immunoproapoptotic molecule scFv-Fdt-tBid modified mesenchymal stem cells for prostate cancer dual-targeted therapy. Cancer Lett. 402, 32–42.

9. Melo, S.A., Luecke, L.B., Kahlert, C., Fernandez, A.F., Gammon, S.T., Kaye, J., LeBleu, V.S., Mittendorf, E.A., Weitz, J., Rahbari, N., et al. (2015). Glypican-1 identifies cancer exosomes and detects early pancreatic cancer. Nature 523, 177–182.

10. De Silva, N., Samblas, M., Martínez, J.A., and Milagro, F.I. (2018). Effects of exosomes from LPS-activated macrophages on adipocyte gene expression, differentiation, and insulin-dependent glucose uptake. J. Physiol. Biochem. 74, 559–568.

11. Xu, B., Niu, X., Zhang, X., Tao, J., Wu, D., Wang, Z., Li, P., Zhang, W., Wu, H., Feng, N., et al. (2011). miR-143 decreases prostate cancer cells proliferation and migration and enhances their sensitivity to docetaxel through suppression of KRAS. Mol. Cell. Biochem. *350*, 207–213.

12. Chu, H., Zhong, D., Tang, J., Li, J., Xue, Y., Tong, N., Qin, C., Yin, C., Zhang, Z., and Wang, M. (2016). A functional variant in miR-143 promoter contributes to prostate cancer risk. Arch. Toxicol. *90*, 403–414.

13. Panigrahi, G.K., Ramteke, A., Birks, D., Abouzeid Ali, H.E., Venkataraman, S., Agarwal, C., Vibhakar, R., Miller, L.D., Agarwal, R., Abd Elmageed, Z.Y., and Deep, G. (2018). Exosomal microRNA profiling to identify hypoxia-related biomarkers in prostate cancer. Oncotarget *9*, 13894–13910.

14. Datta, A., Kim, H., Lal, M., McGee, L., Johnson, A., Moustafa, A.A., Jones, J.C., Mondal, D., Ferrer, M., and Abdel-Mageed, A.B. (2017). Manumycin A suppresses exosome biogenesis and secretion via targeted inhibition of Ras/Raf/ERK1/2 signaling and hnRNP H1 in castration-resistant prostate cancer cells. Cancer Lett. *408*, 73–81.

15. Ramteke, A., Ting, H., Agarwal, C., Mateen, S., Somasagara, R., Hussain, A., Graner, M., Frederick, B., Agarwal, R., and Deep, G. (2015). Exosomes secreted under hypoxia enhance invasiveness and stemness of prostate cancer cells by targeting adherens junction molecules. Mol. Carcinog. *54*, 554–565.

16. Marote, A., Teixeira, F.G., Mendes-Pinheiro, B., and Salgado, A.J. (2016). MSCs-Derived Exosomes: Cell-Secreted Nanovesicles with Regenerative Potential. Front. Pharmacol. *7*, 231.

17. Alcayaga-Miranda, F., González, P.L., Lopez-Verrilli, A., Varas-Godoy, M., Aguila-Díaz, C., Contreras, L., and Khoury, M. (2016). Prostate tumor-induced angiogenesis is blocked by exosomes derived from menstrual stem cells through the inhibition of reactive oxygen species. Oncotarget *7*, 44462–44477.

18. Tokar, T., Pastrello, C., Rossos, A.E.M., Abovsky, M., Hauschild, A.C., Tsay, M., Lu, R., and Jurisica, I. (2018). mirDIP 4.1-integrative database of human microRNA target predictions. Nucleic Acids Res. *46* (D1), D360–D370.

19. Lewis, B.P., Burge, C.B., and Bartel, D.P. (2005). Conserved seed pairing, often flanked by adenosines, indicates that thousands of human genes are microRNA targets. Cell *120*, 15–20.

20. Agarwal, V., Bell, G.W., Nam, J.W., and Bartel, D.P. (2015). Predicting effective microRNA target sites in mammalian mRNAs. eLife *4*, e05005.

21. Niu, X.B., Fu, G.B., Wang, L., Ge, X., Liu, W.T., Wen, Y.Y., Sun, H.R., Liu, L.Z., Wang, Z.J., and Jiang, B.H. (2017). Insulin-like growth factor-I induces chemoresistance to docetaxel by inhibiting miR-143 in human prostate cancer. Oncotarget *8*, 107157–107166.

22. Hoshina, S., Sekizuka, T., Kataoka, M., Hasegawa, H., Hamada, H., Kuroda, M., and Katano, H. (2016). Profile of Exosomal and Intracellular microRNA in Gamma-Herpesvirus-Infected Lymphoma Cell Lines. PLoS ONE *11*, e0162574.

23. Anand, S., Samuel, M., Kumar, S., and Mathivanan, S. (2019). Ticket to a bubble ride: Cargo sorting into exosomes and extracellular vesicles. Biochim. Biophys (Acta Proteins Proteom). Published online February 26, 2019. https://doi.org/10.1016/j.bbapap.2019.02.005.

24. Li, I., and Nabet, B.Y. (2019). Exosomes in the tumor microenvironment as mediators of cancer therapy resistance. Mol. Cancer *18*, 32.

25. Chinenov, D.V., Rapoport, L.M., Shpot, E.V., Enikeev, D.V., Chernov, Y.N., Taratkin, M.S., and Korolev, D.O. (2018). Comparative results of cryoablation and laparoscopic radical prostatectomy in the treatment of localized prostate cancer. Urologia *85*, 68–72.

26. Sprinkart, A.M., Marx, C., Träber, F., Block, W., Thomas, D., Schild, H., Kukuk, G.M., and Mürtz, P. (2018). Evaluation of Exponential ADC (eADC) and Computed DWI (cDWI) for the Detection of Prostate Cancer. RoFo Fortschr. Geb. Rontgenstr. Nuklearmed. *190*, 758–766.

27. Sturge, J., Caley, M.P., and Waxman, J. (2011). Bone metastasis in prostate cancer: emerging therapeutic strategies. Nat. Rev. Clin. Oncol. *8*, 357–368.

28. Chi, K.N., Bjartell, A., Dearnaley, D., Saad, F., Schröder, F.H., Sternberg, C., Tombal, B., and Visakorpi, T. (2009). Castration-resistant prostate cancer: from new pathophysiology to new treatment targets. Eur. Urol. *56*, 594–605.

29. Rodríguez, M., Bajo-Santos, C., Hessvik, N.P., Lorenz, S., Fromm, B., Berge, V., Sandvig, K., Linē, A., and Llorente, A. (2017). Identification of non-invasive miRNAs biomarkers for prostate cancer by deep sequencing analysis of urinary exosomes. Mol. Cancer *16*, 156.

30. Kumar, B., Rosenberg, A.Z., Choi, S.M., Fox-Talbot, K., De Marzo, A.M., Nonn, L., Brennen, W.N., Marchionni, L., Halushka, M.K., and Lupold, S.E. (2018). Cell-type specific expression of oncogenic and tumor suppressive microRNAs in the human prostate and prostate cancer. Sci. Rep. *8*, 7189.

31. Park, K., Chiu, Y.L., Rubin, M.A., Demichelis, F., and Mosquera, J.M. (2013). V-ets erythroblastosis virus E26 oncogene homolog (avian)/Trefoil factor 3/high-molecular-weight cytokeratin triple immunostain: a novel tissue-based biomarker in prostate cancer with potential clinical application. Hum. Pathol. *44*, 2282–2292.

32. Guo, J., Sun, M., Teng, X., and Xu, L. (2017). MicroRNA-7-5p regulates the expression of TFF3 in inflammatory bowel disease. Mol. Med. Rep. *16*, 1200–1206.

33. Hirahata, M., Osaki, M., Kanda, Y., Sugimoto, Y., Yoshioka, Y., Kosaka, N., Takeshita, F., Fujiwara, T., Kawai, A., Ito, H., et al. (2016). PAI-1, a target gene of miR-143, regulates invasion and metastasis by upregulating MMP-13 expression of human osteosarcoma. Cancer Med. *5*, 892–902.

34. Zhong, W., He, B., Zhu, C., Xiao, L., Zhou, S., and Peng, X. (2013). [MiR-143 inhibits migration of human nasopharyngeal carcinoma cells by negatively regulating GLI3 gene.] Nan Fang Yi Ke Da Xue Xue Bao *33*, 1057–1061.

35. Furuta, T., Miyaki, S., Ishitobi, H., Ogura, T., Kato, Y., Kamei, N., Miyado, K., Higashi, Y., and Ochi, M. (2016). Mesenchymal Stem Cell-Derived Exosomes Promote Fracture Healing in a Mouse Model. Stem Cells Transl. Med. *5*, 1620–1630.

36. Gonzalez-King, H., García, N.A., Ontoria-Oviedo, I., Ciria, M., Montero, J.A., and Sepúlveda, P. (2017). Hypoxia Inducible Factor-1α Potentiates Jagged 1-Mediated Angiogenesis by Mesenchymal Stem Cell-Derived Exosomes. Stem Cells *35*, 1747–1759.

37. Calderón, A., Ortiz-Espín, A., Iglesias-Fernández, R., Carbonero, P., Pallardó, F.V., Sevilla, F., and Jiménez, A. (2017). Thioredoxin (Trxo1) interacts with proliferating cell nuclear antigen (PCNA) and its overexpression affects the growth of tobacco cell culture. Redox Biol. *11*, 688–700.

38. Strzalka, W., and Ziemienowicz, A. (2011). Proliferating cell nuclear antigen (PCNA): a key factor in DNA replication and cell cycle regulation. Ann. Bot. *107*, 1127–1140.

39. Huang, C.F., Teng, Y.H., Lu, F.J., Hsu, W.H., Lin, C.L., Hung, C.C., Tung, J.N., Hsieh, Y.H., and Liu, C.J. (2017). β-mangostin suppresses human hepatocellular carcinoma cell invasion through inhibition of MMP-2 and MMP-9 expression and activating the ERK and JNK pathways. Environ. Toxicol. *32*, 2360–2370.

40. Cao, H., Yu, H., Feng, Y., Chen, L., and Liang, F. (2017). Curcumin inhibits prostate cancer by targeting PGK1 in the FOXD3/miR-143 axis. Cancer Chemother. Pharmacol. *79*, 985–994.

41. Zhou, P., Chen, W.G., and Li, X.W. (2015). MicroRNA-143 acts as a tumor suppressor by targeting hexokinase 2 in human prostate cancer. Am. J. Cancer Res. *5*, 2056–2063.

42. Rickman, D.S., Chen, Y.B., Banerjee, S., Pan, Y., Yu, J., Vuong, T., Perner, S., Lafargue, C.J., Mertz, K.D., Setlur, S.R., et al. (2010). ERG cooperates with androgen receptor in regulating trefoil factor 3 in prostate cancer disease progression. Neoplasia *12*, 1031–1040.

43. Perera, O., Evans, A., Pertziger, M., MacDonald, C., Chen, H., Liu, D.X., Lobie, P.E., and Perry, J.K. (2015). Trefoil factor 3 (TFF3) enhances the oncogenic characteristics of prostate carcinoma cells and reduces sensitivity to ionising radiation. Cancer Lett. *361*, 104–111.

44. Liu, J., Li, M., Wang, Y., and Luo, J. (2017). Curcumin sensitizes prostate cancer cells to radiation partly via epigenetic activation of miR-143 and miR-143 mediated autophagy inhibition. J. Drug Target. *25*, 645–652.

45. Zheng, Y., Yang, F., Fu, L., and Liu, K. (2018). The mechanism of miR-143 inducing apoptosis of liver carcinoma cells through regulation of the NF-κB pathway. Oncol. Lett. *15*, 9567–9571.

46. Ma, Z., Luo, Y., and Qiu, M. (2017). miR-143 Induces the Apoptosis of Prostate Cancer LNCap Cells by Suppressing Bcl-2 Expression. Med. Sci. Monit. *23*, 359–365.

47. Li, P., Kaslan, M., Lee, S.H., Yao, J., and Gao, Z. (2017). Progress in Exosome Isolation Techniques. Theranostics *7*, 789–804.

48. Théry, C., Amigorena, S., Raposo, G., and Clayton, A. (2006). Isolation and characterization of exosomes from cell culture supernatants and biological fluids. Curr. Protoc. Cell Biol., *Chapter 3*, Unit 3.22.
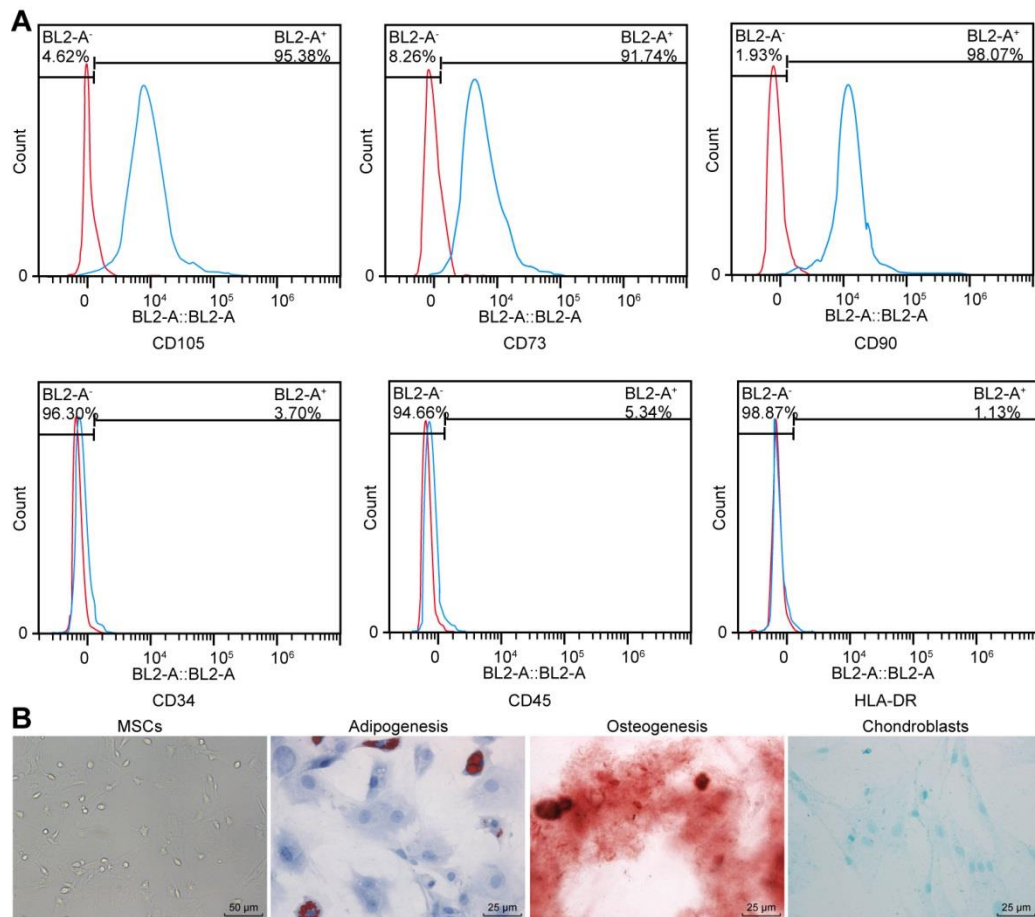
Supplemental Information

Exosomes Derived from miR-143-Overexpressing

MSCs Inhibit Cell Migration and Invasion

in Human Prostate Cancer by Downregulating TFF3

Yuanyuan Che, Xu Shi, Yunpeng Shi, Xiaoming Jiang, Qing Ai, Ying Shi, Fengyan Gong, and Wenyan Jiang

Supplementary figure 1. Identification of BMSCs. A. BMSCs characterization detected using flow cytometry; the cells were positive for CD105, CD73 and CD90 and negative for CD34, HLA-DR and CD45. B, representative images of BMSCs under the light microscope (scale bar = 50 μM); adipogenic (left), osteogenic (middle) and chondroblasts (right) differentiation abilities measured using Oil Red O staining and Alizarin Red staining (scale bar = 25 μM). BMSCs, human bone-marrow derived mesenchymal stem cells.